MAGNETIC COUPLING BETWEEN DC TACHOMETER AND MOTOR AND ITS EFFECT ON MOTION CONTROL

Shorya Awtar
Kevin C. Craig

Department of Mechanical Engineering, Aeronautical Engineering and Mechanics
Rensselaer Polytechnic Institute, Troy, NY12180, USA

Abstract: This paper presents an accurate tachometer model that takes into account the effect of magnetic coupling in a DC motor-tachometer assembly. Magnetic coupling arises due to the presence of mutual inductance between the tachometer winding and the motor winding (a weak transformer effect). Tachometer feedback is widely used for servo-control of DC motors, which can suffer from closed-loop instability due to the presence of compliant components in the drive system. It is essential to have an accurate sensor model to predict and address these resonance related problems. The inadequacy of the conventional tachometer model, which treats the DC tachometer as a 'gain', is pointed out. The exact tachometer model identified in this paper is incorporated in the modeling of a system that has multiple flexible elements, and is used for parameter identification and feedback motion control. The effect of the tachometer dynamics on controller design is discussed in terms of system poles and zeros.

1. INTRODUCTION

Closed-loop servo control of DC motor-load systems is a very common industrial and research application. Very often DC tachometers are used to provide velocity feedback for motion control (McLean, 1978; Ogata, 1998). In the presence of flexible elements in the system, e.g., a compliant motor-load shaft or a flexible coupling, this exercise in servo control becomes quite involved since finite stiffness can cause close-loop instability leading to high frequency ringing (Welch, 1992). This is a highly undesirable phenomenon that can be eliminated by means of appropriate controller design. But, to be able to predict and eliminate this high-frequency resonance problem, it is essential to have an accurate model for the entire system including the sensor.

There are papers in the literature that discuss the control system design for systems with mechanical flexibilities in terms of colocated and noncolocated controls (Cannon, 1984; Franklin, 1994). Most of these discussions assume that a 'perfect' position or velocity signal is available for feedback and that sensor dynamics is negligible. Such an assumption might be acceptable for routine applications, but can become questionable for high-performance applications.

The conventional tachometer model (McLean, 1978) does not recognize any sensor dynamics and treats the tachometer as a simple 'gain'. When high-speed and high-precision motion control is desired using an integrated motor-tachometer assembly, the conventional model proves to be of little use in predicting the system response for high frequencies. This paper presents an accurate tachometer model that takes into account the effect of a weak mutual inductance between the tachometer winding and motor winding. This magnetic coupling phenomenon leads to noticeable sensor dynamics. The exact tachometer dynamics thus identified is then incorporated in the modeling of a system that has multiple shaft flexibility, and is used for parameter identification and feedback motion control.

Predictions using this new model are in excellent agreement with experimental results.

It is found that the above-mentioned tachometer dynamics introduces some additional zeros in the open-loop transfer function of the system, which can significantly influence the controller design for eliminating closed instability.

2. EXPERIMENTAL SET-UP

To study and analyse the close-loop instability problem in DC motor servo systems, an experimental test set-up, which consists of an integrated permanent magnet DC motor-tachometer unit, is assembled. A voltage-to-current PWM servo amplifier is employed to operate the motor in current mode. The system input is in the form of motor current. The system output, which is the tachometer signal, may be used for system identification or for feedback motion control.

The objective of this set-up is to obtain frequency response plots for the system described above. A DSP software/hardware tool, SigLab is used to send a sine sweep over a user-specified frequency range as the system input in the form of a voltage signal to the current amplifier. At the same time SigLab also collects the system output, which is the tachometer voltage in this case. Based on this input-output data, SigLab constructs the frequency response plots for the system. A schematic of this set-up is shown in Fig. 1.

3. CONVENTIONAL D.C. TACHOMTER AND ITS INEFFICACY

Consider a DC motor-tachometer assembly. A shaft of finite stiffness, K, connects the tachometer armature and the motor armature. For this initial test, the motor shaft is not connected to an external load. A physical model of the system with lumped parameters is shown in Fig. 2.

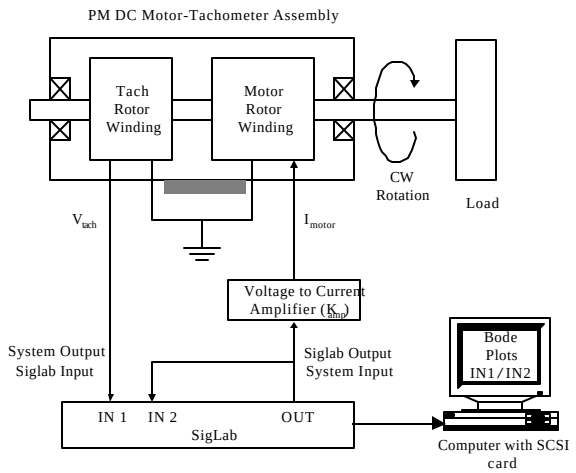

Fig.1. Schematic of Experimental Set-up

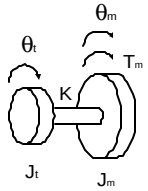

Fig. 2. Physical model of motor-tachometer assembly

By drawing free-body diagrams for the two inertias J_t and J_m, and applying Newton's Second Law, we obtain the following transfer function,

$$\frac{q_t}{T_m} = \frac{K}{s^2\,[J_t\,J_m s^2 + K(J_t + J_m)]} \tag{3.1}$$

In the derivation of the above transfer function all frictional losses (Coulomb, viscous and structural) have been neglected. Being small, these dissipation terms do not dictate the presence of poles and zeros.

Using the conventional electrical models for DC motor and tachometer commonly found in textbooks,

$$\begin{aligned} T_m &= K_{t\_motor}\ i_m \\ V_{tach} &= K_{b\_tach}\ \dot{q}_t \end{aligned} \tag{3.2}$$

to model the motor and tachometer system described in Section 2. Hence the overall system transfer function is,

$$\frac{V_{tach}}{V_{in}} = \frac{K_{amp}\ K_{b\_tach}\ K_{t\_motor}\ K}{s\,[\,J_t\ J_m\ s^2 + K\ (J_t + K_m)\,]} \tag{3.3}$$

Table 1. List of symbols used in this paper

Variable/Parameter	Motor	Tachometer
Angular position	θ_m	θ_t
Armature inertia	J_m	J_t
Permanent Magnet Stator Field	$\mathbf{B_{m1}}$	$\mathbf{B_{m2}}$
Armature Field	$\mathbf{B_{a1}}$	$\mathbf{B_{a2}}$
Armature Current	I_1	I_2
Torque Constant	K_{t_motor}	K_{t_tach}
Torque generated	T_m	T_{tach}
Flux linkage in Armature Coil due its own Current	Φ_1	Φ_2
Area Vector of Armature Coil (pointing in the same direction as the armature field)	$\mathbf{A_1}$	$\mathbf{A_2}$
Armature Resistance	R_1	R_2
Armature Inductance	L_1	L_2
Number of Armature Coils	N_1	N_2
Angular velocity of the Armature	ω_m	ω_{tach}
Back emf Constant / Generator Constant	K_{b_motor}	K_{b_tach}

The analytical frequency response for this transfer function is compared to the experimental frequency response plots, obtained using SigLab.

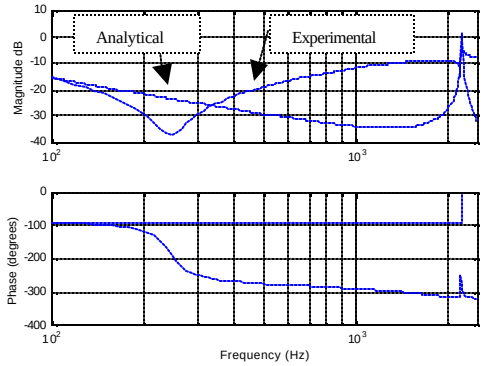

Fig. 3 V_{tach}/V_{in}: Comparison of analytical and experimental frequency response plots for the motor-tachometer system

The following observations can be made from the above comparison plots:

1. The analytically predicted results match the experimental results in the low frequency range (< 100Hz).
2. For higher frequencies the experimental results distinctly deviate from the predicted results and hence the system model breaks down in the high frequency range.
3. The experimental results indicate the presence of two pairs of complex-conjugate zeros in the system transfer function that are not predicted at all by the analysis.
4. The experimental results reveal one complex-conjugate pole pair and this is very close to the pole predicted by the analysis.
5. In the experimental plot, a phase drop of 180^o is noticed at the first zero frequency. This implies that the corresponding complex conjugate zero pair lies on right side of the imaginary axis in the s-plane.

In the above analysis, expressions (3.2) represent textbook models of idealized 'electromagnetically isolated' motor and tachometer respectively, which may be over-simplifications. Therefore, to resolve the discrepancies observed, a thorough investigation to find a more accurate model for the integrated motor-tachometer assembly is carried out.

4. INTEGRATED MOTOR-TACHOMETER ASSEMBLY: A NEW ELECTRICAL MODEL

Consider an integrated motor-tachometer assembly where the both the armatures are mounted closely on the same shaft (Fig. 4). In general, there can be an angular offset between the motor stator field and the tachometer stator field, say α in this case.

We notice that the armature field of the motor produces a flux linkage in the tachometer winding and similarly the armature field of the tachometer produces a certain flux linkage in the motor winding,

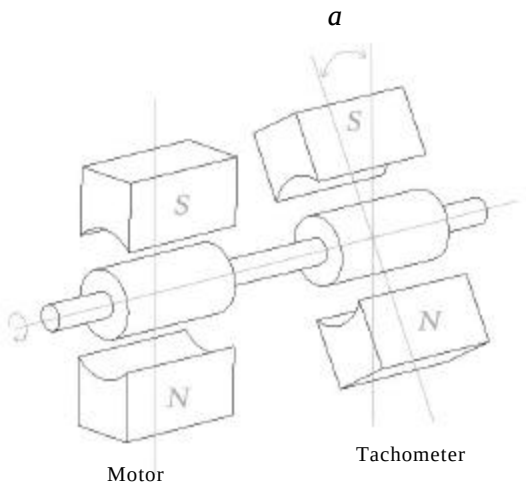

Fig. 4 Angular orientations of the Motor and Tachometer permanent magnets

which in effect leads to mutual inductance between the two coils. This effect is better understood from Fig. 5, which shows all the fields that play a role in the motor-tachometer interaction.

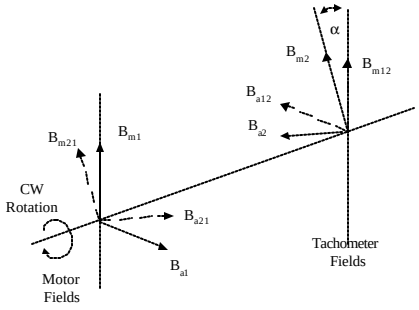

Fig. 5 Motor and tachometer fields

In Fig. 5, the respective permanent magnet stator fields, $\mathbf{B_{m1}}$ and $\mathbf{B_{m2}}$, and the armature fields, $\mathbf{B_{a1}}$ and $\mathbf{B_{a2}}$, of the motor and tachometer are indicated. Directions of $\mathbf{B_{m1}}$ and $\mathbf{B_{m2}}$ are defined by the orientation of permanent magnet stators. For clockwise rotation of the rotors, directions of $\mathbf{B_{a1}}$ and $\mathbf{B_{a2}}$, as shown in the figure, can be derived assuming perfect commutation in the motor and tachometer. These directions are fixed in space. Since the two devices are not magnetically insulated, the tachometer armature (coil 2) sees a weak field, $\mathbf{B_{a12}}$, due to the motor armature current. Thus, $\mathbf{B_{a12}}$ is the magnetic field due to motor armature current (I_1) experienced by the tachometer armature (coil 2). $\mathbf{B_{a12}}$ is in the same plane as $\mathbf{B_{a1}}$, but is opposite in direction. The tachometer also experiences the effect of the permanent magnets of the motor. This appears in the form of a weak field $\mathbf{B_{m12}}$, resulting from the leakage flux of the permanent magnets of the motor. $\mathbf{B_{m12}}$ is in the same direction as $\mathbf{B_{m1}}$. Similar arguments holds true for the motor winding as well, e.g., $\mathbf{B_{a21}}$ is the magnetic field due to tachometer armature current (I_2) experienced by the motor armature (coil 1). All the fields experienced by the motor and the tachometer coils are summarized in the following vector diagrams.

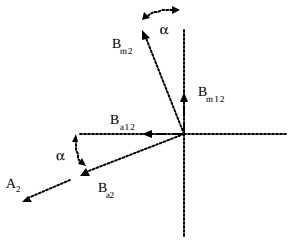

Fig. 6 Magnetic Fields present in the Tachometer

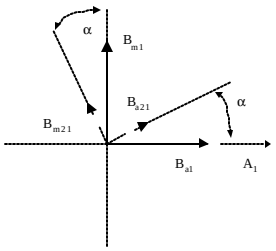

Fig. 7 Magnetic Fields present in the Motor

It is observed that the effect of $\mathbf{B_{m12}}$ on the tachometer equations is negligible. It does not lead to any dynamic effects; it only changes the stator field that the tachometer armature rotates in, by a small amount. This in turn only causes a little change in the torque constant and the generator/tachometer constant. Similarly, $\mathbf{B_{m21}}$ is of little consequence in the motor equation.

The magnitudes of the armature fields are linearly dependent on the respective armature currents. Therefore the following holds,

$$\begin{aligned} B_{a1} &= k_1 I_1 \\ B_{a21} &= k_{21} I_2 \\ B_{a2} &= k_2 I_2 \\ B_{a12} &= k_{12} I_1 \end{aligned} \tag{4.1}$$

where k_1, k_2, k_{12} and k_{21} are constants.

The presence of the armature fields $\mathbf{B_{a12}}$ and $\mathbf{B_{a21}}$ leads to mutual inductance between the two coils. Fig. 8 illustrates the weak transformer effect between the two armature coils. The situation, though, is very different from an ideal transformer. There is no core between the two coils, the permeability of air is very low, and most part of the flux linked with each coil is leakage flux and mutual flux is small.

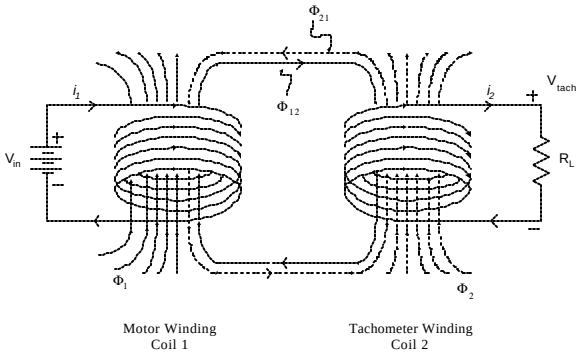

Fig.8 Transformer effect between the two coils

In Fig. 8,
$\Phi_{?}$ is the flux linkage in coil 1 due to I_1
$\Phi_{2?}$ is the flux linkage in coil 1 due to I_2
Φ_2 is the flux linkage in coil 2 due to I_2
Φ_{12} is the flux linkage in coil 2 due to I_1

Referring to Figures 6 and 7, and expressions (4.1), it is seen that,

$$\begin{aligned} \Phi_1 &= \vec{B}_{a1} \cdot \vec{A}_1 = (k_1 I_1) A_1 \\ \Phi_2 &= \vec{B}_{a2} \cdot \vec{A}_2 = (k_2 I_2) A_2 \\ \Phi_{21} &= \vec{B}_{a21} \cdot \vec{A}_1 = (k_{21} I_2) A_1 \cos(a) \\ \Phi_{12} &= \vec{B}_{a12} \cdot \vec{A}_2 = (k_{12} I_1) A_2 \cos(a) \end{aligned} \tag{4.2}$$

Consequently, the resultant flux linkage in motor armature = $\Phi_1 + \Phi_{21}$ and, the resultant flux linkage in tachometer armature = $\Phi_2 + \Phi_{12}$. Applying KVL and Ohm's Law to the electrical circuit comprising coil 1, i.e. the motor armature, we get

$$V_{in} - V_{backemf} - N_1 \frac{d(\Phi_1 + \Phi_{21})}{dt} = R_1 I_1 \tag{4.3}$$

As is evident from the above equation, there are two effects that oppose V_{in}: a back emf that arises due to the armature motion in the stator field ($\mathbf{B_{m1}}$ and $\mathbf{B_{m21}}$) and an induced emf due to the inductance of the armature coil (self-inductance as well as mutual inductance). Both these effects are impeding effects, which is reflected by the negative sign associated with them (Lenz's Law). Similarly, the application of KVL and Ohm's Law to the electrical circuit containing the tachometer armature (coil 2) in Fig. 8, leads to

$$V_b - N_2 \frac{d(\Phi_2 + \Phi_{12})}{dt} = (R_2 + R_L) I_2 \tag{4.4}$$

Inductances can be defined using expressions (4.2),

$$\begin{aligned} N_1\Phi_1 &= N_1(K_1 I_1) A_1 \triangleq L_1 I_1 \\ N_2\Phi_2 &= N_2(K_2 I_2) A_2 \triangleq L_2 I_2 \\ N_1\Phi_{21} &= N_1(K_{21} I_2) A_1 \cos(a) \triangleq M_{21} I_2 \cos(a) \\ N_2\Phi_{12} &= N_2(K_{12} I_1) A_2 \cos(a) \triangleq M_{12} I_1 \cos(a) \end{aligned} \tag{4.5}$$

L_1 and L_2 are the self-inductance values for the motor and tachometer coils respectively. M_{12} (=M_{21}) is the mutual inductance value between the motor and tachometer coils, when $\alpha = 0^o$. Furthermore, it can be shown easily that,

$$\begin{aligned} V_{backemf} &= K_{b\_motor} w_m \\ V_b &= K_{b\_tach} w_{tach} \end{aligned} \tag{4.6}$$

Using these results, motor equation (4.3) reduces to,

$$V_{in} - K_{b\_motor} w_m - L_1 \frac{d I_1}{dt} - M_{21} \cos(a) \frac{d I_2}{dt} = R_1 I_1 \tag{4.7}$$

and the tachometer equation (4.4) reduces to,

$$K_{b\_tach}\, w_{tach} - L_2 \frac{d\, I_2}{dt} - M_{12}\cos(a)\frac{d\, I_1}{dt} = (R_2 + R_L)\, I_2 \tag{4.8}$$

The tachometer terminal voltage measured by an external device, is given by $R_L I_2$,

$$\begin{aligned} V_{tach} &= R_L\, I_2 \\ &= K_{b\_tach}\, w_{tach} - L_2 \frac{d\, I_2}{dt} - M_{12}\cos(a)\frac{d\, I_1}{dt} - R_2\, I_2 \end{aligned} \tag{4.9}$$

This is the enhanced tachometer model that includes the effect of mutual inductance between motor and tachometer armatures, which is ignored in the conventional model. Torque models for the motor and tachometer are relatively simple. The retarding torque produced by the tachometer, the torque generated by the motor, and the overall torque output from the motor-tachometer assembly, are respectively given by

$$\begin{aligned} T_{tach} &= K_{t\_tach}\, I_2 \\ T_m &= K_{t\_motor}\, I_1 \\ T_{out} &= K_{t\_motor}\, I_1 - K_{t\_tach}\, I_2 \end{aligned} \tag{4.10}$$

Equations (4.7) through (4.10) are the final results of this derivation. At this stage certain simplifications can be considered. Since the input impedance of the voltage-measuring device (e.g. SigLab) is usually very high, the load current I_2 is much smaller than the motor current I_1. We can therefore eliminate terms containing I_2, wherever it occurs in equations (4.7)-(4.10). At this point however, the term '$-R_2\, I_2$' in the V_{tach} expression (4.9) is retained. This is done to resolve a singularity in the analytical frequency plots. Since this term constitutes a damping term, the sign associated with it is critical in determining the phase change at the corresponding zero and pole frequencies. In the absence of this term, the model faces a singularity and arbitrarily assigns either a $+180^o$ or -180^o phase change. A damping term, however small (even negligible), resolves this ambiguity and determines whether this phase change has to be $+180^o$ or -180^o, depending upon the sign associated with it. Thus, this term is retained only to predict the phase plot in frequency response. It has negligible effect on the magnitude plot.

A final observation is made regarding the '$-R_2\, I_2$' term. Had the transformer effect been an ideal one,, the relationship $I_2 = (N_1/N_2)\, I_1$ would hold. In the present case, this is not true since the transformer effect is a weak one. Nevertheless, I_2 may be weakly related to I_1 by some empirical constant. Based on this argument, '$R_2\, I_2$' may be replaced by '$K_r\, I_1$' where K_r is an experimentally determined empirical constant. The validity of this empirical conjecture is confirmed later by experimental measurements.

The motor-tachometer equations thus reduce to,

$$\begin{aligned} &\text{Motor:} && V_{in} - K_{b\_motor}\, w_m - L_1 \frac{d\, I_1}{dt} = R_1\, I_1 \\ &\text{Tach:} && V_{tach} = K_{b\_tach}\, w_{tach} + K_m \frac{d\, I_1}{dt} - K_r\, I_1 \\ &\text{Torque:} && T_{out} = K_{t\_motor}\, I_1 \end{aligned} \tag{4.11}$$

where the constants K_m and K_r are defined as,

$K_m \triangleq -M_{12}\cos(a)$ (magnetic coupling constant)

$K_r \triangleq R_2\ (I_2 / I_1)$ (loading effect constant)

Comparing these results with the previous results (3.2), it can be noticed that while the motor model and the torque expression remain the same, the tachometer model has additional terms. Note that since the tachometer is magnetically coupled to the motor, the motor current influences the tachometer terminal voltage despite the fact that the two are electrically insulated. The new tachometer model reduces to the conventional model if the magnetic coupling constant K_m = 0, and the loading effect constant K_r = 0. These two constants are easily determined experimentally, as shall be described in the next section. K_r is always positive, while K_m may be positive or negative depending on the angle α.

5. EXPERIMENTAL VERIFICATION OF THE NEW MODEL

The new tachometer model obtained in Section 4 can now be incorporated in the analysis for the same motor-tachometer system that was studied earlier in Section 3. The overall transfer function for the motor-tachometer electromechanical system using the new tachometer model can be shown to be,

$$\begin{aligned} \frac{V_{tach}}{V_{in}} &= \frac{K_{amp}\,[K_m\,(den)\,s^2 - K_r\,(den)\,s + K_{t\_motor} K_{b\_tach} K]}{(den)\,s} \\ (den) &\triangleq [J_t\, J_m\, s^2 + K\,(J_t + J_m)] \end{aligned} \tag{5.1}$$

This analytically obtained transfer function for the tachometer-motor system is used to generate the frequency response plots in MATLAB. These are then compared with the experimentally obtained plots (Fig. 9).

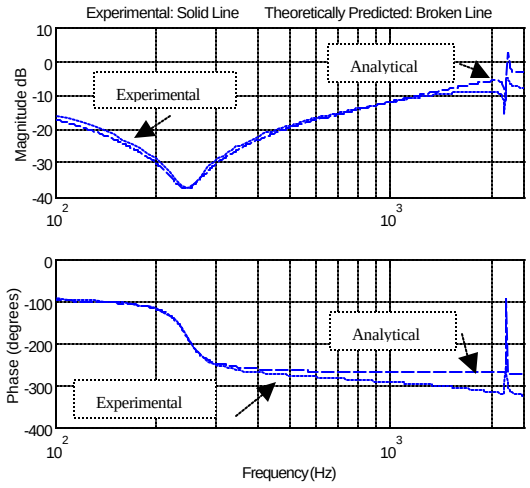

Fig. 9 V_{tach}/V_{in}: Comparison of analytically predicted (using the new model) and experimentally obtained frequency response plots for the motor-tachometer system.

It is interesting to note that the new model accurately predicts the experimental observations even for the high frequency range. Although the conventional model predicted the system poles accurately, it failed to explain the presence of system zeros. The new model addresses resolves this inconsistency very satisfactorily. Some interesting observations made from the above comparison are:

1. Looking at the system transfer function given by equation (5.1), the presence of the additional zeros can now be explained. The most noticeable enhancement in the new tachometer model is the presence of a magnetic coupling constant, K_m. It is evident that a positive K_m leads to complex conjugate zero pairs in the system. Clearly, these zeros will disappear for K_m=0. Because of this magnetic coupling term, the denominator of the system transfer function finds a place in the numerator, hence the additional zeros that appear are strongly dependent on the system poles
2. The presence of K_r with a negative sign explains why the phase drops by 180^o at the first zero frequency. The loading effect pushes the first complex-conjugate pole pair to the right side of the imaginary axis on the s-plane.

Since K_m and K_r are completely dependent on geometry and experimental set-up, they are best determined experimentally. Thus, once the new tachometer model is experimentally confirmed, the results of the above experimental plots are then used to back-calculate and tune the values of these unknown parameters K (shaft stiffness), K_m (magnetic coupling constant) and K_r (loading effect constant). K_m and K_r are found to be very small numbers.

6. TYPICAL MOTION CONTROL APPLICATION

Now a typical problem in DC motor motion control using tachometer feedback is considered. The same integrated motor-tachometer assembly described in Section 2 is used. The motor shaft, in this case, is connected to a load by means of a flexible coupling of known stiffness. Furthermore the load is in the form of two inertia's connected by a shaft. Thus the system has multiple flexible elements (Fig.10)

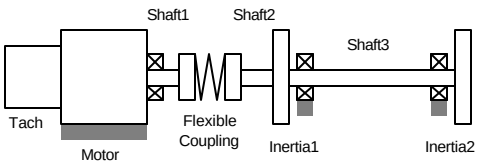

Fig. 10 Motor-tachometer-load System

A lumped parameter model is used to describe the above system, with the assumption that dissipation terms (i.e. Coulomb friction, viscous damping and material damping) are small enough that they do not influence the existence of system poles and zeros. The purpose of the present investigation is to identify the poles and zeros of the overall system that arise due to its mechanical and electromagnetic attributes, and mechanical damping has little influence on these. At a later stage though, an empirical amount of damping is added at all the poles and zeros, so as to avoid ambiguities in the predicted phase plots (as was discussed in Section 4). A physical model of the above system is shown below,

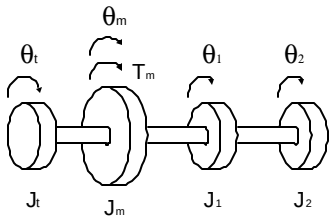

Fig.11 Physical Model of the motor-tachometer-load system

The following transfer function for the mechanical system can be easily obtained

$$\frac{q_t}{T_m} = \frac{[num]}{s^2 \cdot [den]} \tag{6.1}$$

where,

$$[num] = K\,[J_1 J_2 s^4 + (J_1 K_2 + J_2 K_1 + J_2 K_2) s^2 + K_1 K_2]$$

$$\begin{aligned}[den] = {} & s^6 [J_t J_m J_1 J_2] + \\ & s^4 [K_2 J_t J_m J_1 + K_1 J_t J_m J_2 + K_2 J_t J_m J_2 + \\ & \quad K J_m J_1 J_2 + K J_t J_1 J_2 + K_1 K_t J_1 J_2] + \\ & s^2 [K_1 K_2 J_t J_m + K K_2 J_1 J_m + K K_1 J_2 J_m \\ & \quad K K_2 J_2 J_m + K K_2 J_t J_1 + K K_1 J_t J_2 \\ & \quad K K_2 J_t J_2 + K_1 K_2 J_t J_1 + K K_1 J_1 J_2 + K_1 K_2 J_1 J_2] \\ & + [K K_1 K_2 (J_t + J_m + J_1 + J_2)]\end{aligned}$$

Using the motor model and the new tachometer model presented in Section 4, the overall transfer function of the electromechanical system can be shown to be,

$$\frac{V_{tach}}{V_{in}} = \frac{K_{amp}\,[K_m s^2\,(den) - K_r\, s\,(den) + K_{t\_motor}\, K_{b\_tach}\,(num)]}{s\,(den)} \tag{6.2}$$

On the other hand, if the conventional tachometer model were used, the overall system transfer function would be given by,

$$\frac{V_{tach}}{V_{in}} = \frac{K_{amp}\, K_t\, K_{tach}\,(num)}{s\,(den)} \tag{6.3}$$

Comparing these two transfer functions, it is clear that the new model captures some dynamics that is missing in the old model. It is note-worthy that, if K_r and K_m are set to zero in expression (6.2), then it reduces to (6.3). The analytical responses predicted by these two models are compared with experimental measurements.

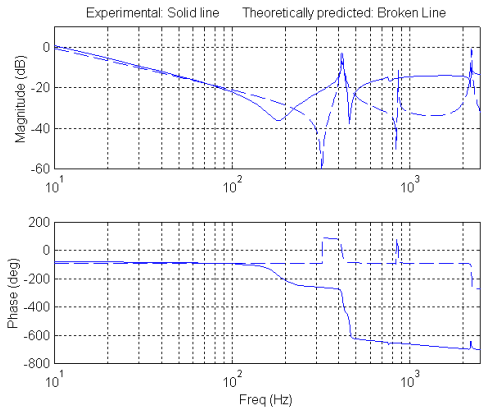

Fig. 12 V_{tach}/V_{in}: Comparison of experimental frequency response and predicted frequency response using conventional tachometer model

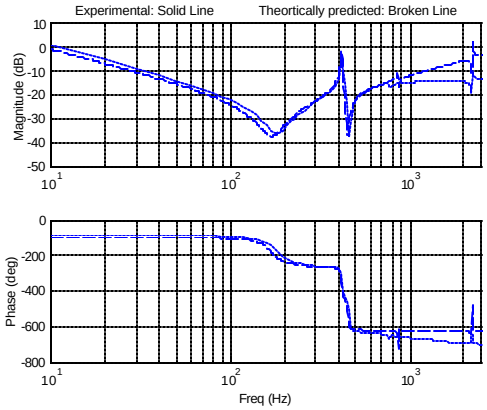

Fig. 13 V_{tach}/V_{in}: Comparison of experimental frequency response and predicted frequency response using the proposed tachometer model

Clearly the conventional model is inadequate for predicting the high-frequency system response. The tachometer dynamics adds zeros to the system and also pushes some of the system zeros to the right side of s-plane. This is obvious from the phase drop at zero frequencies.

Thus the overall system model, with the new tachometer model incorporated, can be now used for System Identification and Control System Design. An experiment similar to the one described above can be carried out for the purpose of parameter identification. Each of the complex conjugate pole pairs in the system transfer function represents a resonance mode of the system arising from the flexible elements (e.g., compliant shaft, flexible coupling etc.). Thus if the stiffness of some flexible member is unknown and can't be measure directly, it can be easily back-calculated from the pole frequency locations obtained from experimental data and an accurate knowledge of the complete system model. This was done in Section.5, where the exact motor-tachometer shaft stiffness was estimated from the frequency response plots.

Apart from parameter identification, the new tachometer model has significant implications in terms of controller design for achieving close-loop stability. If the time-response requirements are not very stringent, a lead controller works well as long as the crossover frequency is kept low enough. But this severely limits the close-loop bandwidth. On the other hand, if high speed servo-control is desired, the tachometer dynamics becomes critical in the design of a compensator for the system. A benign aspect of the tachometer dynamics is that it introduces a zeros close to each pole making it look like a colocated controls problem. But this benefit is offset by the fact that the tachometer renders the system non-minimum phase by pushing the system zeros into the right-hand side of the s-plane. This makes the control problem very demanding, because instead of adding phase to the system the zeros now deplete the phase of the system. Therefore, unless a compensator that can provide a large phase is used, the closed-loop system speed is limited. Hence the tachometer has an overall detrimental effect on the closed loop stability of the system in discussion. Any controller that is designed for such a servo-control system should recognize the sensor dynamics and should be able to compensate for it.

REFERENCES

Cannon, R.H. Jr., and D.E. Rosenthal (1984). Experiments in Control of Flexible Structures with Noncolocated Sensors and Actuators. *Journal of Guidance*, **Vol.7**, pp. 546-553

Fitzgerald, A.E. and C. Kingsley. (1961). *Electric Machinery: The Dynamics and Statics of Electromechanical Energy Conversion*. McGraw-Hill Book Company, New York.

Franklin, G.F. and D.J. Powell (1994). *Feedback Control of Dynamic Systems*. Addison-Wesley Publishing Company, New York.

McLean, D. (1978). Mathematical Models of Electrical Machines. *Measurement and Control*, **Vol. 11**, pp. 231-236.

Ogata, K. (1998). *Modern Control Engineering*. Prentice-Hall, New Delhi.

Sen, P.C. (1989). *Principles of Electric Machines and Power Electronics*. John Wiley & Sons, New York.

Welch Jr., R.H. (1992). Mechanical Resonance in a Closed Loop Servo System, Tutorial for Motion Control Expo.